International Research Journal of Advanced Engineering and Science
ISSN (Online): 2455-9024

Research on the Mechanical Behavior of the Reduction Gear Assembly in XCB Tracked Vehicle Powertrain System

Hoang Van Thu[1], Duong Xuan Bien[2,*]
[1]Z179 Mechanical Engineering Company Limited, Hanoi, Vietnam
[2]Advanced Technology Center, Le Quy Don Technical University, Hanoi, Vietnam

Abstract - *This paper presents the results of the computational design and fabrication of the XCB tracked vehicle side reduction gear assembly. The reduction gear assembly is part of the vehicle's power transmission system and serves to increase torque on the drive wheel axles. The planetary gear set is the main component of the reduction gear. Planetary gear sets are widely used in heavy-duty mechanical systems requiring high power density, good concentricity, and high durability. In this study, a single-stage planetary gear set is investigated based on design parameters to evaluate the main mechanical behavior of the gears under high load and high speed conditions. Specifically, meshing forces, tooth root bending strength, tooth surface contact stress, and safety factors are determined. Additionally, the influence of changing tooth width on stress values and safety factors is also considered. The results of this study provide a basis for evaluating the working conditions and lifespan of planetary gear sets in particular, and reduction gear sets in general, on the powertrain system of the XCB tracked vehicle.*

Keywords - *Tracked vehicles, reduction gears, planetary gear sets, meshing force, stress.*

I. INTRODUCTION

Tracked vehicles are ground vehicles that use tracks wrapped around the load wheels, steering wheels, and drive sprocket to generate traction. This configuration helps reduce ground contact pressure (due to the large contact area), increases the ability to overcome soft/rough terrain, and provides better traction than wheeled vehicles in many conditions [1]. This type of vehicle has the great advantage of terrain mobility (mud/sand) and good ability to climb slopes and overcome obstacles, and stability when carrying heavy loads (suitable for heavy combat vehicles) [2]. However, typical limitations of this type of vehicle are internal mechanical losses (track joint friction, roller-track friction, etc.), noise, vibration, high maintenance costs, and high track wear; when operating on hard roads, it can cause increased wear and fuel consumption. The main characteristic of the tracked vehicle's drive system is the strong integration of steering, braking, and transmission functions with differential wheel systems and the ability to create a large speed and torque difference between the left and right tracks instead of the wheel angle steering mechanism like wheeled vehicles [3]. Tracked vehicle systems have been researched and developed for a long time with the accumulation of experience and overcoming limitations and shortcomings in each specific design and manufacturing stage. The successful research, design, manufacturing, and testing of tracked vehicles will affirm the research, design, and manufacturing capabilities of all types of armored vehicles in general and infantry fighting vehicles in particular of defense industry facilities to all countries in the world. Typical tracked vehicles such as the XCB infantry fighting vehicle are integrated, advanced military vehicles with the participation of many technologies from many different fields: from mechanics, chemicals to electronics, control, optics, ...

The powertrain system on tracked vehicles can basically be described in the following drive sequence: engine (diesel or turbine or hybrid), gearbox, steering assembly, output drive, drive wheel and track. In which, the gearbox for tracked vehicles is usually a specialized type because it not only changes gears, but also distributes power to the left-right branches and assists in creating a speed difference for steering [4]. For example, the M113 (APC) vehicle system has maintenance/operation documents describing the powertrain and related assemblies at the technical detail level (unit-level maintenance, steering shaft gear assembly, etc.) [5]. Currently, there are increasingly more studies modeling powertrain-vehicle dynamics and differential steering control (especially with hydrostatic/electric-hybrid drives) to improve cornering stability and performance [6].

In tracked vehicles, the reduction gear is the most important component and is usually located in the final drive and placed on the left/right sides near the drive wheel. Its main function is to reduce the large speed (increase torque) from the output shaft of the drive to the drive wheel. At the same time, it withstands terrain impact loads and transmits stable force to the track [7]. The final drive of tracked vehicles often uses a planetary gear set because it needs a large gear ratio in a narrow space [8]. Furthermore, this set has the ability to divide the load (many gears mesh together) to increase durability and withstand large torque. Therefore, planetary gear structures are very common in reduction gear stages on tracked vehicles. On the other hand, in many architectures, the final drive with a reduction gear not only reduces speed but is also the final mechanical link to effectively implement acceleration - braking - steering states through the transmission of left/right torque.

Gears play a crucial role in mechanical systems, where their strength and performance significantly affect the performance of machinery. Understanding bending stress in gears requires consideration of factors such as load distribution, material properties, and gear geometry. Calculation standards provide guidance for determining

Hoang Van Thu and Duong Xuan Bien, "Research on the mechanical behavior of the reduction gear assembly in the XCB tracked vehicle powertrain system," *International Research Journal of Advanced Engineering and Science*, Volume 11, Issue 1, pp. 33-40, 2025.

bending stress, balancing accuracy and practical applicability through simplified methods based on research and experimental data. Calculation standards provide guidance for determining bending stress in gears using simplified methods, ensuring a balance between accuracy and practicality, based on a large volume of research and data. The AGMA 2001-D04 [9] and ISO 6336-3 [10] standards provide detailed guidance for evaluating the load-carrying capacity of spur and helical gears. JIS B 1701-1 [11] and GB/T 3480-2008 [12] standards provide regional guidelines, consistent with design and manufacturing practices in each country. The accuracy and reliability of gear stress calculations depend strongly on the continuous development and improvement of design standards. Methods for calculating bending stress according to ISO 6336:2006, AGMA 2001-D04, finite element analysis using ANSYS, and strain gauge measurement techniques were compared by Timothy et al. [13], thereby showing the need for continuous improvement of design standards. A small load created by the transmission clearance can optimize the load applied to the roller and maximize bearing life [14]. The bearings applied with this technique and combined with the planetary gear shaft have helped improve the coaxiality of the planetary gear train and the load distribution characteristics. The semi-integrated planetary bearing design also increases the load-carrying capacity of the transmission. Design calculations in [15], [16] have allowed the prediction that the planetary gear reducer has a three-fold longer life than the original gearbox. The adverse effects of rotor torque on the load distribution capability of the planetary gear train and predicted fatigue life, as well as the risk of bearing slippage under low torque conditions for the drive system are described in [17], [18].

As a core component of power transmission systems in advanced equipment, planetary gear sets play an irreplaceable role in aerospace, tracked vehicles, and wind turbine systems. Their transmission accuracy and reliability face serious challenges under harsh operating conditions, such as wide temperature ranges, heavy loads, and high speeds [19-21]. Designs for planetary gear sets with two series-connected stages and one high-speed parallel shaft stage are described in [22]. Accordingly, gear sets with three, four, and five planetary gears all provide good load distribution and sufficiently large transmission ratios. The research results also show that technologies related to materials (high-purity steel used for bearings and gears), planetary gear design (using elastic structures to improve load distribution between gears), bearing design (adjusting roller convexity to allow for greater coaxial misalignment), integrating inner ring gears into planetary gears, using hydrodynamic bearings, and gearbox architecture (increasing the number of planetary gears, optimally selecting the gear ratio for each stage, using thin-walled planetary gear racks, and combined planetary gear stages) all allow for a continuous increase in power density. Analytical methods provide a balance between computational efficiency and accuracy by using simplified models to calculate the bending stress of gears. Based on experimental data and classical mechanics, these methods play a vital role in establishing gear design standards. Nicoletto's early studies [23] used complex potentials to analyze gear tooth stress, laying the groundwork for later more advanced models. Kapovich and Shekhtman [24] introduced direct gear design to minimize bending stress through geometric optimization, marking a shift toward more precise design. Kawalec et al. [25] compared tooth root strength using ISO and AGMA standards combined with FEM verification, thereby highlighting the importance of analytical models in gear stress analysis. Arikan [26], [27] provided analytical expressions for the AGMA geometric coefficient J of external spur gears, providing a basis for gear stress analysis. Li [28], [29] studied the influence of errors and corrective measures on the contact and bending strength of spur gears, highlighting the impact of manufacturing and assembly errors. Pedersen [30] improved the bending stress calculations through asymmetric gears and shape optimization, showing the potential for reducing gear stress through design improvements.

This paper focuses on calculating the meshing force components based on the input parameters of gear reducers in general and planetary gear transmissions in particular. The main mechanical behaviors determined include tooth surface contact stress, tooth root bending stress, and corresponding safety factors. Based on the calculation results, the safety and ability to meet the requirements of the transmission are confirmed. Furthermore, the tooth root width is also identified as a key factor in evaluating changes in mechanical behavior indicators.

II. Materials and Methods

A. Modeling of the reduction gear assembly

The reduction gear assembly is in the form of a planetary gear set consisting of 1 central gear (Sun), 3 planetary gears (Planet), and a fixed differential housing (Ring) (Fig. 1). Accordingly, the type of gear set considered is a single-stage, straight-toothed planetary gear set.

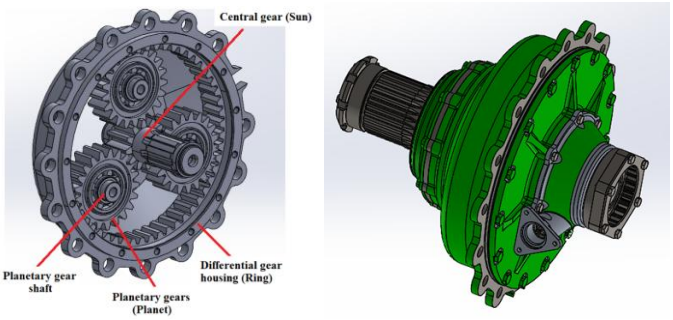

Fig. 1. Gear reducer on XCB tracked vehicle

The input parameters for evaluating the mechanical behavior of the system are described in Tab. 1 and Tab. 2.

The drive engine under consideration is a 6-cylinder, 4-stroke, V-type UTD-20 diesel engine with direct fuel injection, water cooling, multi-fuel, a displacement of 15.8 liters, and a power output of 300 HP (or 224 kW) at a maximum speed of 2600 rpm. The mechanical behavior evaluation problem is as follows: based on the input design parameters, determine the transmission parameters of the system, the meshing forces, contact stresses, and bending

Hoang Van Thu and Duong Xuan Bien, "Research on the mechanical behavior of the reduction gear assembly in the XCB tracked vehicle powertrain system," *International Research Journal of Advanced Engineering and Science*, Volume 11, Issue 1, pp. 33-40, 2025.

stresses at the meshing points of the transmission. From this, determine the safety factors and draw conclusions about the initial design parameters. Furthermore, regarding important geometric parameters that determine the transmission's performance, such as tooth width and adjustment coefficient, how will changing these affect the stress, safety factor, and lifespan of the system? This also needs to be considered and analyzed in detail.

Tab. 1. Basic parameters of the transmission system

Parameters	Symbols	Values	Units
Gear ratio	i	5.5	
Tooth module	m	6	mm
Engine angle	α	20	Degree
Number of planetary gears	n_P	3	Piece
Number of teeth on the central gear	Z_S	12	Tooth
Number of teeth on the planetary gears	Z_P	21	Tooth
Number of teeth on the differential gears	Z_R	54	Tooth
Tooth width	b	43	mm

Tab. 2. Operating conditions of the transmission system

Parameters	Symbols	Values	Units
Maximum torque	$T_{\max}$	5250	Nm
Maximum output speed	n_c	950	rpm
Planetary gear mechanical efficiency	η	0.97	
Load distribution coefficient between planetary gears	K_γ	1.2	
Total load coefficient (grade 7 tooth quality, enclosed operation) normal and maximum	$K, K_{\max}$	1.35 ; 1.55	
Planetary and central gear materials	18XGT - GOST 453-71		
Fixed differential gear materials	40XM - GOST 453-71		
Gear hardness		55-60	HRC
Bending stress limits for different materials	$\sigma_{F,\lim}$	600	MPa
Contact stress limits for different materials	$\sigma_{H,\lim}$	1800	MPa

B. Calculation and mechanical analysis of the gearbox assembly

1) Determine the drive system parameters

The pitch circle diameters of the gears are determined as follows

$$d = m \times Z \quad (1)$$

Accordingly, the pitch circle diameter of the central gear is presented as follows

$$d_S = m \times Z_S = 6 \times 12 = 72(mm) \quad (2)$$

The pitch circle diameter of the planetary gear is calculated as follows

$$d_P = m \times Z_P = 6 \times 21 = 126(mm) \quad (3)$$

The pitch circle diameter of the differential gear (inner ring gear) is described as follows

$$d_R = m \times Z_R = 6 \times 54 = 324(mm) \quad (4)$$

The center distance between the center gear and the planetary gear is calculated as follows

$$a_{SP} = \frac{m(Z_S + Z_P)}{2} = 99(mm) \quad (5)$$

The center distance between the planetary gear and the fixed differential gear is determined as follows

$$a_{SP} = \frac{m(Z_R - Z_P)}{2} = \frac{6(54-21)}{2} = 99(mm) \quad (6)$$

The output torque of the center gear is determined as follows

$$T_S = \frac{T_{\max}}{\eta \times i} = \frac{5250}{0.97 \times 5.5} \approx 984(Nm) \quad (7)$$

Comparing the V-UTD 20 Diesel engine specifications with the rated power $P = 224(kW), n = 2600(rpm)$, the rated torque in the highest speed range is described as follows

$$T_{def} = \frac{P}{\omega_{\max}} = \frac{P}{2\pi(\frac{2600}{60})} \approx 823(Nm) \quad (8)$$

Comparing T_S and T_{def}, we find a better match in terms of torque when the central shaft is limited to speed $n_c \le 950(rpm)$. In other words, at low speeds, the torque value can reach a higher level than at high speeds.

2) Determine the meshing forces at the center gears and planetary gears

The total tangential meshing force on the planetary gears is determined [31], [32]:

$$F_t = \frac{2T_S}{d_S} = \frac{2 \times 984}{0.072} \approx 27335(N) \quad (9)$$

When distributing the load onto each planetary gear, it should be noted that, due to manufacturing and assembly errors in practice, this load distribution does not guarantee absolute uniformity on each planetary gear. Therefore, it is necessary to add a load unevenness coefficient K_γ [33], [34]. This value is usually in the range (1.1 to 1.25). In this case, with 3 planetary gears, each gear is supported by 2 bearings and the tooth accuracy reaches level 7, so choose $K_\gamma = 1.2$. At this time, the tangential meshing force for each gear is calculated as follows

$$F_{t,P} = K_\gamma \frac{F_t}{3} = 1.2 \times \frac{27335}{3} \approx 10934(N) \quad (10)$$

The normal meshing force corresponding to each planetary gear is determined as follows

$$F_{n,P} = \frac{F_{t,P}}{\cos\alpha} = \frac{10934}{\cos 20^0} \approx 11636(N) \quad (11)$$

The radial engagement force corresponding to each planetary gear is calculated as follows

$$F_{r,P} = F_{t,P} \times \tan\alpha = 10934 \times \tan 20^0 \approx 3980(N) \quad (12)$$

3) Determining the bending stress of the tooth root

According to Lewis's formula (basic form) [35], [36], [37] when each tooth is viewed as a cantilever beam. At this time, the approximate bending stress is determined as follows

$$\sigma_F \approx \frac{F_{t,P} \times K}{b \times m \times Y} \quad (13)$$

In which, K is the combined load factor (including basic assumptions about dynamic factors, light impact and stress distribution according to tooth width). Accordingly, the empirical value is usually taken as $K = 1.35$. The tooth form factor is Y. This factor depends on the number of teeth, the

Hoang Van Thu and Duong Xuan Bien, "Research on the mechanical behavior of the reduction gear assembly in the XCB tracked vehicle powertrain system," *International Research Journal of Advanced Engineering and Science*, Volume 11, Issue 1, pp. 33-40, 2025.

International Research Journal of Advanced Engineering and Science
ISSN (Online): 2455-9024

adjustment factor and the meshing angle [38], [39], [40]. With meshing angle $\alpha = 20^0$, this value can be determined as follows

$$Y \approx 0.484 - \frac{2.87}{Z} \quad (14)$$

Accordingly, for the central gear, this value is determined as follows $Y_S \approx 0.484 - \frac{2.87}{Z_S} = 0.2448$, and with planetary gears: $Y_P \approx 0.484 - \frac{2.87}{Z_P} = 0.3473$. At this point, the bending stress of the central tooth root is calculated as follows

$$\sigma_{F,S} \approx \frac{F_{t,P} \times K}{b \times m \times Y_S} \approx 233.68(MPa) \quad (15)$$

The bending stress value of the planetary gear root is determined as follows

$$\sigma_{F,P} \approx \frac{F_{t,P} \times K}{b \times m \times Y_P} \approx 164.74(MPa) \quad (16)$$

It is easy to see that the flexural strength of the central and planetary gears is much smaller than the flexural strength limit of the corresponding material $\sigma_{F,\lim} = 600(MPa)$. Thus, the design shows that the parameters ensure the flexural strength condition [41].

4) Determine the contact stress of the tooth surface

The calculation of contact strength according to tooth surface can be determined according to Hertz and AGMA standards [34] as follows

$$\sigma_H \approx Z_E \sqrt{\frac{F_{t,P} \times K}{b \times d \times I}} \quad (17)$$

Trong đó, Z_E là hệ số đàn hồi (phụ thuộc vào hệ số Young (E), Poison (ν) ứng với vật liệu chế tạo bánh răng). I là hệ số hình học tiếp xúc, giá trị này có thể lấy theo tiêu chuẩn AGMA 908-B89 [34]. Với cặp bánh răng ăn khớp ngoài - ngoài (Trung tâm và hành tinh) thì cặp vật liệu tương ứng là Thép-Thép, do đó có thể lấy $E = 210(GPa), \nu = 0.3$. Lúc này, hệ số đàn hồi Z_E được xác định:

In which, Z_E is the elastic coefficient (depending on the Young's coefficient (E), Poison coefficient (ν) corresponding to the gear material). I is the contact geometry coefficient, this value can be taken according to the AGMA 908-B89 standard [34]. For external-external meshing gears (center and planetary), the corresponding material pair is Steel-Steel, so $E = 210(GPa), \nu = 0.3$ can be taken. At this time, the elastic coefficient Z_E is considered as follows

$$Z_E \approx \sqrt{\frac{1}{2\pi(\frac{1-\nu^2}{E})}} \approx 191.6 \quad (18)$$

For center gears with pitch circle diameter $d = d_S = 72(mm)$ and tooth ratio $m_G = \frac{Z_P}{Z_S} = \frac{21}{12} = 1.75$, a preliminary value of $I \approx 0.102$ can be selected. Accordingly, the tooth surface contact stress of the planetary gear and center gear pair (outer-outer contact) is calculated as follows

$$\sigma_{H,SP} \approx Z_E \sqrt{\frac{F_{t,P} \times K}{b \times d_S \times I}} = 191.6 \sqrt{\frac{10934 \times 1.35}{43 \times 72 \times 0.102}} \approx 1309.94(MPa)$$

For a fixed planetary gear and differential gear pair (outer-inner contact), with pitch circle diameter $d = d_P = 126(mm)$ and tooth ratio $m_G = \frac{Z_R}{Z_P} = \frac{54}{21} = 2.571$, a preliminary value $I \approx 0.116$ can be selected. In this case, the surface contact stress of the planetary gear-differential gear pair is determined as follows

$$\sigma_{H,PR} \approx Z_E \sqrt{\frac{F_{t,P} \times K}{b \times d_P \times I}} = 191.6 \sqrt{\frac{10934 \times 1.35}{43 \times 126 \times 0.116}} \approx 928.55(MPa) \quad (19)$$

The contact stress values are smaller than the limiting contact stress value $\sigma_{H,\lim} = 1800(MPa)$. Therefore, the design parameters ensure contact strength.

5) Determine the load on the planetary gear shafts and the safety factor

In the planetary gear set of the reducer, the differential housing is fixed so the bearing and shaft loads of the planetary gears are governed by the radial meshing force component [42] created by the two meshing operations (planet with differential and planet with center). Therefore, the preliminary load acting on the planetary gear bearing is determined [43]:

$$F_{Pin} \approx 2 \times F_{r,P} = 2 \times 3980 = 7960(N) \quad (20)$$

Each bearing has 2 rows so the load is also evenly distributed across the bearings with the following values [14]:

$$F_{bering} = \frac{F_{Pin}}{2} = 3980(N) \quad (21)$$

With the load value acting on the bearing just determined, the size of the straight roller bearing can be selected according to its service life and accompanying standards. The safety factor for tooth root bending is determined as follows

$$n_F = \frac{\sigma_{F,\lim}}{\sigma_{F,S}} = \frac{600}{233.5} \approx 2.57 \quad (22)$$

The tooth surface contact safety factor is determined as follows

$$n_H = \frac{\sigma_{H,\lim}}{\sigma_{H,SP}} = \frac{1800}{1309.9} \approx 1.37 \quad (23)$$

C. Investigating the influence of tooth width and offset coefficient on the mechanical behavior of a transmission

From Eq. (17), the tooth surface contact stress depends on many different quantities. Assuming the parameters $Z_E, F_{t,P}, K, d$ have fixed values. The contact geometry coefficient can be modeled according to the following rule [32]:

Hoang Van Thu and Duong Xuan Bien, "Research on the mechanical behavior of the reduction gear assembly in the XCB tracked vehicle powertrain system," *International Research Journal of Advanced Engineering and Science*, Volume 11, Issue 1, pp. 33-40, 2025.

$$I(x_S) = I_0(1 + k_I x_S) \quad (24)$$

In which, x_S is the profile shift coefficient of the center gear, I_0 is the geometric contact coefficient when $x_S = 0$, and k_I is the sensitivity coefficient describing the increase of I according to x_S. It should be noted that positive shift usually makes the geometric contact line more suitable for contact stress because the radius of curvature is larger and the slip of the meshing surface is reduced [44]. Thus, from Eq. (17), the contact stress value can be completely investigated corresponding to the change of the tooth width value (b). Specifically:

$$\sigma_H = Z_E \sqrt{\frac{(\frac{K_\gamma}{n_P}) \times (\frac{2}{d_S/1000}) \times (\frac{T_{\max}}{\eta \times i}) \times K}{b \times d_S \times I_0(1 + k_I x_S)}} \quad (25)$$

From Eq. (24), the contact safety factor can be determined as follows

$$n_H = \frac{\sigma_{H,\lim}}{\sigma_{H,SP}} = \frac{\sigma_{H,\lim}}{Z_E} \sqrt{\frac{b \times d_S \times I(x_S)}{F_{t,P} \times K}} \quad (26)$$

Replacing Eq. (25) with Eq. (27), this coefficient is calculated as follows

$$n_H = \frac{\sigma_{H,\lim}}{Z_E} \sqrt{\frac{b \times d_S \times I_0(1 + k_I x_S)}{(\frac{K_\gamma}{n_P}) \times (\frac{2}{d_S/1000}) \times (\frac{T_{\max}}{\eta \times i}) \times K}} \quad (27)$$

Some key observations can be preliminarily determined as follows:

- The tooth contact stress is inversely proportional to the square root of the value of b. conversely, the safety factor is directly proportional to the square root of the value of b, meaning:

$$\sigma_H \propto \frac{1}{\sqrt{b}}; n_H \propto \sqrt{b} \quad (28)$$

- Thus, as the value of b increases, the safety factor increases and the tooth surface contact stress decreases. For the adjustment factor xs corresponding to the selected sensitive model [45], the relationship of contact stress and contact safety factor is determined as follows

$$\sigma_H \propto \frac{1}{\sqrt{I(x_S)}} = \frac{1}{\sqrt{I_0(1 + k_I x_S)}}; \quad n_H \propto \sqrt{I_0(1 + k_I x_S)} \quad (29)$$

- Positive adjustment will also increase the safety factor, but this value increases as a function of the square root. The bending stress and safety factor of the tooth root are determined similarly as follows

$$\sigma_F = \frac{K}{b \times m \times Y} \times \frac{K_\gamma}{n_P} \times \frac{2}{d_S/1000} \times \frac{T_{\max}}{\eta \times i} \quad (30)$$

And,

$$n_F = \sigma_{F,\lim} \times b \times m \times Y \times \frac{\eta \times i \times n_P}{2 \times K \times K_\gamma} \times \frac{d_S}{T_{\max}} \quad (31)$$

The Y-shaped bending geometry coefficient with adjustment depends only on the number of teeth and the profile adjustment coefficient xs. In particular, the profile adjustment coefficient strongly influences the root thickness, root fillet radius, and critical cross-sectional position. In this case, the effective bending geometry coefficient is considered as follows

$$Y_{eff}(x_S) = Y_0(1 + c_F x_S) \quad (32)$$

In which, Y_0 is the base Lewis coefficient (when the adjustment factor $x_S = 0$). c_F is the sensitivity coefficient and takes a positive value when $x_S > 0$ (the tooth root is thickened and the bending strength of the tooth root is increased). At this point, the stress and bending safety factor of the tooth root are determined as follows

$$\sigma_F = \frac{K \times F_{t,P}}{b \times m \times Y_0(1 + c_F x_S)} \quad (33)$$

And,

$$n_F = \frac{\sigma_{F,\lim} \times b \times m \times Y_0(1 + c_F x_S)}{K \times F_{t,P}} \quad (34)$$

Thus, the relationship between stress and contact safety factor with respect to root width and profile adjustment factor can be seen as follows

$$\sigma_F \propto \frac{K}{b(1 + c_F x_S)}; n_F \propto \frac{b(1 + c_F x_S)}{K} \quad (35)$$

As the value of b increases, the tangential stress decreases linearly, and the contact safety factor increases linearly. Similarly, with a correction factor $x_S > 0$, positive correction improves bending strength with increasing root width. With the design parameters described in Tab. 1 and Tab. 2, the influence of root width and profile correction factor on stress and safety factor is shown in Fig. 3, Fig. 4, and Fig. 5. The corresponding values are shown in Tab. 3.

Tab. 3. Stress values and safety factors corresponding to tooth width

b (mm)	σ_F (MPa)	σ_H (MPa)	n_F	n_H
40	251.2085	1353.927	2.388454	1.329466
41	245.0815	1337.313	2.448165	1.345982
42	239.2462	1321.297	2.507877	1.362298
43	233.6823	1305.843	2.567588	1.37842
44	228.3714	1290.918	2.6273	1.394356
45	223.2965	1276.494	2.687011	1.410112
46	218.4422	1262.543	2.746722	1.425694
47	213.7945	1249.04	2.806434	1.441107
48	209.3404	1235.96	2.866145	1.456358
49	205.0682	1223.283	2.925856	1.47145
50	200.9668	1210.989	2.985568	1.486389
51	197.0263	1199.058	3.045279	1.501179
52	193.2373	1187.472	3.10499	1.515825
53	189.5913	1176.216	3.164702	1.530331
54	186.0804	1165.274	3.224413	1.5447
55	182.6971	1154.632	3.284124	1.558938
56	179.4347	1144.277	3.343836	1.573046
57	176.2867	1134.195	3.403547	1.587029
58	173.2472	1124.375	3.463258	1.60089

Hoang Van Thu and Duong Xuan Bien, "Research on the mechanical behavior of the reduction gear assembly in the XCB tracked vehicle powertrain system," *International Research Journal of Advanced Engineering and Science*, Volume 11, Issue 1, pp. 33-40, 2025.

59	170.3109	1114.805	3.52297	1.614631
60	167.4723	1105.476	3.582681	1.628257

Fig. 2a shows that the bending stress and contact stress values decrease as the tooth width increases. The curve shape is linear. The bending stress value decreases more slowly than the contact stress. In terms of value, the bending stress (approximately 170-250 MPa) is much smaller than the contact stress (1100-1350 MPa) as the tooth root width increases. Therefore, when the gearbox operates under heavy load, watertight conditions, and at high speeds, contact failure will be the dominant cause, rather than tooth root bending fracture.

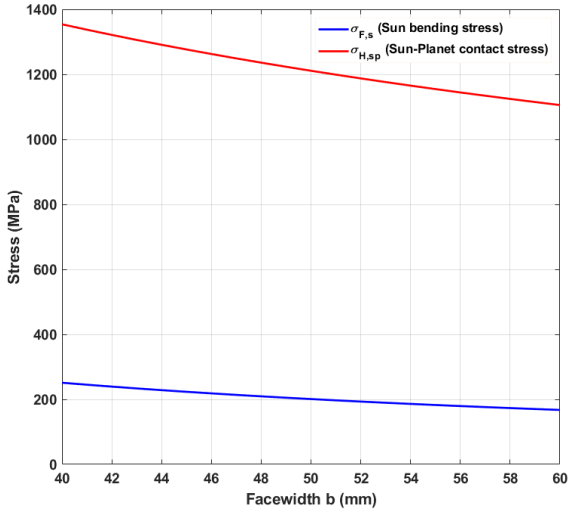

(a)

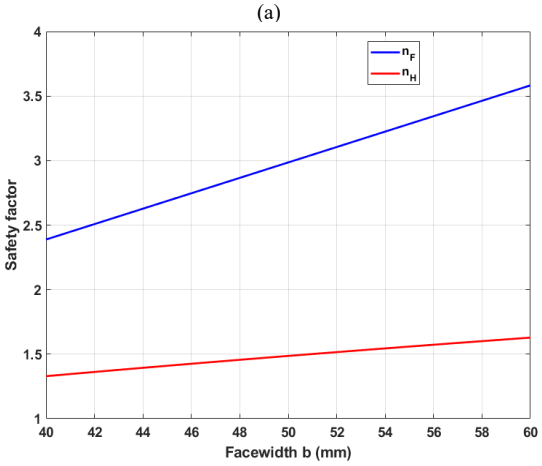

(b)

Fig. 2. Effect of tooth width on stress and safety factor

The safety factor values described in Fig. 2b show that they both increase linearly. The contact safety factor (approximately 1.35 to 1.6) increases more slowly than the bending safety factor (approximately 2.4 to 3.6). Even with $b = 40mm, n_F > 2$, so the gear is very safe in terms of bending; increasing b would not be necessary if only considering bending. However, the value of n_H increases slowly, and at the threshold of n_H in the range of (1.3; 1.4), the gear has a high risk of failure. It can be observed that when increasing b by more than 10mm compared to the design, the bending stress decreases by 20-25%, the contact stress decreases by 10-12%, the bending safety factor increases sharply, while the contact safety factor increases slowly. Clearly, when the tooth width (b) is between 50mm and 55mm, the coefficients $n_F = 3$and $n_H = 1.5$. This is the optimal range of values, both technically and in terms of the operating conditions of the gearbox.

D. Results of manufacturing and practical operation of the gearbox

Based on the evaluation of the gearbox's mechanical behavior against the initial design specifications, the structure fully meets the requirements for tooth root bending strength and contact strength. All safety values are greater than 1.3, and the contact safety factor is significantly higher. Therefore, the transmission fully meets the requirements for operation at high speeds, under heavy loads, and in confined spaces.

The manufacturing of gearbox components must strictly adhere to technological processes and system technical requirements. First, forging, stamping, and rolling technologies are used to create the initial blanks. Forging and stamping aim to create blanks with shapes similar to the final product, thus saving materials, processing time, and improving material properties. In this stage, steel forging technology is used to replace conventional casting technology to increase mechanical properties and product quality. Next, metal cutting and machining methods such as turning, milling, gear grinding, cylindrical grinding, and wire cutting are applied. These methods are characterized by cutting and shaping the product. To improve the accuracy and quality of the product, modern, high-precision equipment such as CNC lathes and CNC milling machines are used. After machining, heat treatment technologies such as carburizing, quenching, tempering, and annealing are implemented. The purpose of these technologies is to improve the mechanical properties of the material, thereby enhancing product quality. Finally, surface treatment technologies such as plating, sandblasting, shot blasting, and painting are used. These surface treatment steps help protect the product surface after manufacturing from environmental impacts and also enhance the product's aesthetics. Plating technology is used to create a zinc oxide layer to protect the surface of steel parts. Sandblasting technology is used to treat the product surface after heat treatment. Some manufacturing results are shown in Fig. 3, Fig. 4, and Fig. 5.

Fig. 3. Shaft and central gear after fabrication

Hoang Van Thu and Duong Xuan Bien, "Research on the mechanical behavior of the reduction gear assembly in the XCB tracked vehicle powertrain system," *International Research Journal of Advanced Engineering and Science*, Volume 11, Issue 1, pp. 33-40, 2025.

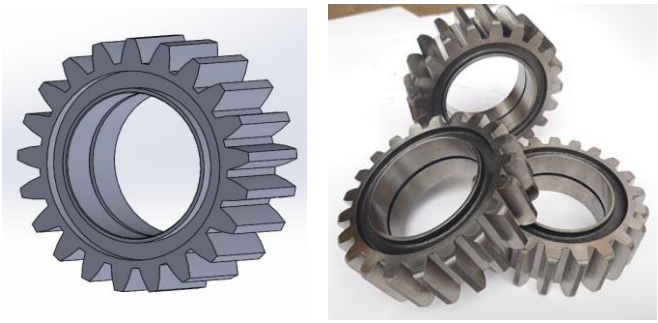

Fig. 4. Planetary gears after fabrication

Fig. 5. Gear reducer after assembly and on the XCB tracked vehicle

III. CONCLUSIONS

This study evaluated the mechanical behavior of a gear reducer in an XCB tracked vehicle powertrain system with the given input design parameters. These behaviors were determined using key criteria including tooth root bending stresses, tooth surface contact stresses, and corresponding safety factors. The influence of tooth root width - one of the most important gear design parameters on mechanical properties - was also investigated in detail. The research results showed that the initial design parameters fully met the criteria for bending strength and contact strength. They met the requirements for high-speed, heavy-load, and watertight operation. Furthermore, increasing the tooth root width increased the transmission's durability with a higher safety factor. Contact stress decreased slowly, and bending stress decreased rapidly with increasing tooth root width, with corresponding reductions of 10-12% and 20-25%. Based on the evaluation results, the transmission system was fabricated and assembled experimentally, fully meeting the initial criteria and requirements. Furthermore, the successful fabrication of the gearbox confirms the ability to master the design and manufacturing technology of the gearbox assembly for the XCB tracked vehicle. All technical features were tested and met the requirements. The products have been assembled onto the vehicle and tested in the field. Initial results ensure the product's technical requirements under real-world working conditions. Moreover, the successful research and fabrication, from calculation and design to manufacturing, contributes to the complete localization of materials and spare parts for the XCB tracked vehicle, reducing dependence on imports from foreign sources.

REFERENCES

[1] Wong, J. Y. (2001). Theory of ground vehicles (3rd ed.). John Wiley & Sons. ISBN 9780471354611

[2] Johnson, C. P. (2012). Comparative analysis of lightweight robotic wheeled and tracked vehicle (Master's thesis). Virginia Polytechnic Institute and State University, Blacksburg, VA.

[3] Han, J., Wang, F., & Wang, Y. (2022). A Control Method for the Differential Steering of Tracked Vehicles Driven Independently by a Dual Hydraulic Motor. Applied Sciences, 12(13), 6355. https://doi.org/10.3390/app12136355

[4] https://www.renk.com/en/products/vehicles/transmissions

[5] U.S. Department of the Army. (2012). TM 9-2520-272-40 (Transmission/Steering related maintenance for M113-family components). NSNlookup.

[6] Qin, Z., Luo, Y., Cao, Z., and Li, K., "A Novel Three-Planetary-Gear Power-Split Hybrid Powertrain for Tracked Vehicles," SAE Technical Paper 2018-01-1003, 2018, https://doi.org/10.4271/2018-01-1003.

[7] RENK Aktiengesellschaft. (n.d.). Technologies for superior mobility: Motion for missions—Transmissions for military tracked vehicles [Technical brochure]. https://www.renk.eu

[8] https://www.renk.com/en/products/vehicles/final-drives

[9] AGMA 2101-D04, Fundamental Rating Factors and Calculation Methods For Involute Spur and Helical Gear Teeth, American Gear Manufacturers Association, Alexandria, VA, 2004.

[10] ISO 6336-3, Calculation of Load Capacity of Spur and Helical gears. Part 3: Calculation of Tooth Bending Strength, International Organization for Standardization, Geneva, Switzerland, 2019 (2019).

[11] JIS B 1701-1, Involute Gear Tooth Profile and Dimensions, Japanese Industrial Standards, Tokyo, Japan, 1973.

[12] GB/T 3480, Calculation of Load Capacity of Spur and Helical Gears, Standards Press of China, Beijing, China, 2021.

[13] J.L. Timothy, B.A. Shaw, R.C. Frazer, External spur gear root bending stress: a comparISOn of ISO 6336:2006, AGMA 2101-D04, ANSYS Finite Element Analysis and Strain Gauge Techniques, Mech. Mach. Theory 111 (2017) 1–9.

[14] Oswald, F.B., E.V. Zaretsky and J.V. Poplawski. 2012. Effect of internal clearance on load distribution and life of radially loaded ball and roller bearings. Tribology Transactions, 55 (2): 245-65. doi: 10.1080/10402004.2011.639050.

[15] Flamang, P. and P. Clement. 2003. Stresses and Load Distribution Factors in Bearings: A Tool to Compare Bearing Alternatives. Dresdner Maschinenelemente Kolloquium, 289-302

[16] Lucas, D. Planet Pac: Increasing Epicyclic Power Density and Performance through Integration (AGMA 05FTM18). AGMA Fall Technical Meeting Proceedings, 2005.

[17] Keller, J. and R. Wallen. 2015. Gearbox Reliability Collaborative Phase 3 Gearbox 2 Test. NREL/TP-5000-63693. National Renewable Energy Laboratory (NREL), Golden, CO (US). doi: 10.7799/1254154. https://doi.org/10.7799/1254154.

[18] Keller, J. and R. Wallen. 2017. Gearbox Reliability Collaborative Phase 3 Gearbox 3 Test. NREL/TP-5000-67612. National Renewable Energy Laboratory (NREL), Golden, CO (US). doi: 10.7799/1337868. https://doi.org/10.7799/1337868.

[19] T. Chen, C. Zhu, J. Chen, H. Liu, A review on gear scuffing studies: theories, experiments and design, Tribol. Int. 196 (2024) 109741, https://doi.org/10.1016/j.triboint.2024.109741.

[20] P. Gao, Q. Yan, H. Liu, C. Xiang, K. Chen, Research on fault characteristics and signal transfer path mechanism of the gear transmission system, Mech. Syst. Signal Process. 228 (2025) 112471, https://doi.org/10.1016/j.ymssp.2025.112471.

[21] K. Feng, J.C. Ji, Q. Ni, M. Beer, A review of vibration-based gear wear monitoring and prediction techniques, Mech. Syst. Signal Process. 182 (2023) 109605, https://doi.org/10.1016/j.ymssp.2022.109605.

[22] ANSI/AGMA 6123-C16, Design Manual for Enclosed Epicyclic Gear Drives

[23] G. Nicoletto, Gear tooth stress analysis by the complex potentials method, Meccanica 27 (1992) 105–110.

[24] A. Kapelevich, Y.V. Shekhtman, Direct gear design: bending stress minimization, Gear Technology 20 (4) (2003) 44–47.

[25] [A. Kawalec, J. Wiktor, D. Ceglarek, Comparative analysis of tooth-root strength using ISO and AGMA Standards in spur and helical gears with FEM-based verification, J. Mech. Des. 128 (5) (2005) 1141–1158.

[26] M.A.S. Arikan, Derivation of analytical expressions for calculation of AGMA geometry factor J for external spur gears, in: Proc. ASME 2001 International Design

[27] Engineering Technical Conferences and Computers and Information in Engineering Conference, Pittsburgh, PA 2B, 2001, pp. 1033–1042.
[28] S. Li, Finite element analyses for contact strength and bending strength of a pair of spur gears with machining errors, assembly errors and tooth modifications, Mech. Mach. Theory 42 (1) (2007) 88–114.
[29] S. Li, Effect of addendum on contact strength, bending strength and basic performance parameters of a pair of spur gears, Mech. Mach. Theory 43 (12) (2008) 1557–1584.
[30] N. Pedersen, Improving bending stress in spur gears using asymmetric gears and shape optimization, Mech. Mach. Theory 45 (2010) 1707–1720.
[31] Cooley, C.G. and R.G. Parker. 2014. A review of planetary and epicyclic gear dynamics and vibrations research. Applied Mechanics Reviews, 66 (4): 040808-1–040804-15. doi: 10.1115/1.4027812.
[32] British Standards Institution, ISO 6336-1:2019: Calculation of load capacity of spur and helical gears - Basic principles, introduction and general influence factors, Mechanical Systems & Components - GBM12, 2019, ISBN 978 0 539 00804 3.
[33] Jonathan Keller, Yi Guo, Zhiwei Zhang, Doug Lucas, Planetary Load Sharing in Three-Point Mounted Wind Turbine Gearboxes: A Design and Test Comparison, Technical Report NREL/TP-5000-67394, April 2017, National Renewable Energy Laboratory 15013 Denver West Parkway Golden.
[34] Hanspeter Dinner, Flexible planet pins for high torque epicyclic gears. Experience with design, manufacturing and application, AGMA Technical Paper, KISSsoft AG – A Gleason Company, American Gear Manufacturers Association 1001 N, 2023.
[35] Lewis, W., 1892. Investigation ofthe strength of gear teeth. Proceedings of the Engineers Club of Philadelphia: 19-23.
[36] Guo, Y., J. Keller and W. LaCava. 2012. Combined Effects of Gravity, Bending Moment, Bearing Clearance, and Input Torque on Wind Turbine Planetary Gear Load Sharing: Preprint. NREL/CP-5000-55968. National Renewable Energy Laboratory (NREL), Golden, CO (US). http://www.nrel.gov/docs/fy12osti/55968.pdf.
[37] https://evolventdesign.com/pages/calculators
[38] Pedrero, J.I., Pleguezuelos, M. and Munoz, M., 2011. Critical stress and load conditions for pitting calculations ofinvolute spur and helical gear teeth. Mechanism and Machine Theory, 46(4), pp. 425–437.
[39] https://www.wmberg.com/resources/blogs/measure-gear-tooth-strength?
[40] Ravindra S. Lahane, H. P. Jawale, Analysis of gear pair contact to pridict efficiency, international journal of advances in production and mechanical engineering, vol 1(5) 2015, pp. 45-59.
[41] British Standards Institution, ISO 6336-6:2019: Calculation of load capacity of spur and helical gears - Calculation of service life under variable load, Mechanical Systems & Components - GBM12, 2019, ISBN 978 0 539 00804 3.
[42] Singh, A., Kahraman, A., and Ligata, H., “Internal Gear Strains and Load Sharing in Planetary Transmissions–Model and Experiments”, J. Mech. Des., 130, pp. 072602, 2008.
[43] LaCava, W., Y. Xing, C. Marks, Y. Guo and T. Moan. 2013. Three-dimensional bearing load share behaviour in the planetary stage of a wind turbine gearbox. IET Renewable Power Generation, 7 (4): 359–69. doi: 10.1049/iet-rpg.2012.0274.
[44] Zaretsky, E.V., D.G. Lewicki, M. Savage and B.L. Vleck. 2007. Determination of turboprop reduction gearbox system fatigue life and reliability. Tribology Transactions, 50 (4), 507-16. doi: 10.1080/10402000701613799.
[45] Budynas, R. G., & Nisbett, J. K. (2020). Shigley’s mechanical engineering design (11th ed.). McGraw-Hill Education.
[46] Ma, Q. and Black, D., "An Accurate Analysis Method to Calculate Planetary Gear Set Load Sharing under Non-Torque Load," SAE Technical Paper 2022-01-0653, 2022, https://doi.org/10.4271/2022-01-0653.